ELSEVIER

Catalysis Today 72 (2002) 267–279

CATALYSIS TODAY

www.elsevier.com/locate/cattod

Plasma-CVD-coated glass beads as photocatalyst for water decontamination

Martin Karches [a], Marcus Morstein [b], Philipp Rudolf von Rohr [a], Roberto L. Pozzo [c], José L. Giombi [c], Miguel A. Baltanás [c,*]

[a] *Department of Mechanical and Process Engineering, Institute of Process Engineering, ETH Zürich, CH-8092 Zürich, Switzerland*
[b] *Laboratory for Surface Science and Technology, Department of Materials, ETH Zürich, CH-8092 Zürich, Switzerland*
[c] *INTEC (Instituto de Desarrollo Tecnológico para la Industria Química), Güemes 3450, S3000GLN Santa Fe, Argentina*

Abstract

Amorphous TiO_2 films were deposited on glass microbeads using a specially designed circulating fluidized bed plasma-CVD reactor. The film thickness was varied between 7 and 120 nm. While only little carbon impurity was found, XPS analysis revealed the presence of silicon, sodium and alkaline earth elements in the titania coating. Reduced amounts of these substrate-originating impurities were observed in the thicker films. By ToF-SIMS imaging, cross-sectional TEM and time-resolved dissolution, the titania coatings were proven to be uniform, both per particle and in terms of the film thickness distribution.

The photocatalytic performance of the composite particles was evaluated in a fully irradiated fluidized-bed photoreactor. The thinnest films had some photocatalytic activity in the as-deposited state, possibly induced by the high specific power of the microwave plasma or silicon doping. The thicker films needed a post-deposition calcination at 723 K to achieve catalytic activity. Both the degree of anatase crystallization and the activity were improved by applying thicker films and after UV irradiation-plus-calcining. All films showed good adhesion and abrasion resistance during the photocatalytic tests. The best plasma-CVD films were about 70% as efficient (per unit reactor volume) as the reference material, P-25 immobilized on quartz sand.

Keywords: CVD; Fluidized bed; Photocatalysis; Plasma; Supported titania

1. Introduction

In the past decade, the use of TiO_2 as a photocatalyst has received much attention in the treatment of wastewater and exhaust gases. For water detoxification, mostly particles in the nanometer range are used, because of their large specific surface area. In slurry reactors, such materials show excellent performance, but it is difficult and expensive, to separate the catalyst from the treated water. To overcome this drawback, titania powder has been immobilized or directly synthesized on supports [1,2]. Together with large two-dimensional surfaces, both compact and highly porous particles, such as silica gel or γ-alumina [3–6], have been used as carriers. Translucent particles of diameters in the 100 μm range are especially well suited, since they allow for efficient use of light, provide a reasonably high surface area and can be used in high mass-transfer reactor systems, such as fluidized beds.

Commercial nanopowder catalysts, such as Degussa P-25, have been fixed onto carrier particles by using

* Corresponding author. Tel.: +54-342-455-9175; fax: +54-342-455-0944.
E-mail address: tderliq@ceride.gov.ar (M.A. Baltanás).

0920-5861/02/$ – see front matter
PII: S0920-5861(01)00505-3

binders and heat treatments [7–10]. An alternative is the in situ synthesis of titania from titanium alcoholate or $TiCl_4$ precursors by wet-chemical [11,12] or chemical vapor deposition (CVD) [13] methods, which is potentially more economic and opens up new ways to optimize the catalyst. Physical vapor deposition processes, such as magnetron sputtering, are successfully used for large-area coatings on flat substrates, but these line-of-sight methods are less suited for the complex surface geometry of particles.

The crystalline anatase phase is preferred for photocatalytic applications [14]. However, titania films produced below 673 K are usually amorphous. Direct formation of anatase at temperatures lower than that has only been reported for SiO_2–TiO_2 composites [5,15], for some low-pressure CVD films [16] and after deposition by an ion-beam method [17]. More commonly, a calcination step at 673–973 K is needed to obtain crystallinity [3,18–21].

Amorphous titania powders prepared by low-temperature plasma-CVD under mild conditions became photocatalytically active after calcination [19]. As described by Korzec et al. [22], amorphous radio frequency (rf) plasma-deposited films were found to be super-hydrophilic, a phenomenon closely correlated to photocatalytic activity [23].

Recently, some of us have demonstrated that plasma-CVD in a circulating fluidized bed (CFB) reactor is a very efficient method to deposit uniform, well-adherent titania coatings on kg-batches of glass beads [24]. Since film thickness has been found to play a dominant role for the photocatalytic activity of titania coatings [21,25,26], we have now coated glass particles with films of different thicknesses. Their ability to oxidize a model compound was investigated using a high performance, 'fully irradiated' fluidized bed photoreactor [8].

2. Experimental

2.1. Catalysts preparation

One-kilogram-batches of soda-lime glass beads ($\langle d \rangle = 124\,\mu m$), pre-treated with 10% HNO_3 to reduce alkali and alkaline earth elements near the surface, were coated in a vacuum-operated CFB plasma-CVD reactor (Fig. 1). The apparatus consists

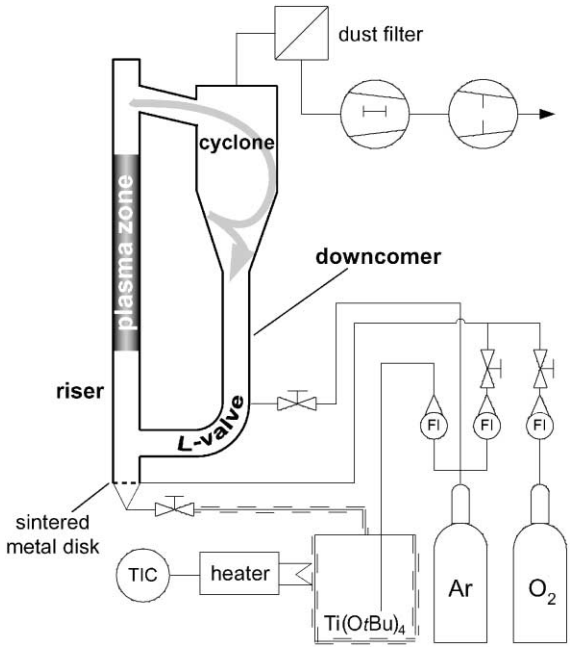

Fig. 1. Schematic of our plasma-CVD apparatus for thin film deposition on particles; the plasma for coating is generated in the riser tube (40 mm i.d.) of a CFB.

of a vertical riser tube (1 m length and 40 mm i.d.), a cyclone for gas/solid separation, a downcomer hose and an aerated L-valve for circulation control. The CFB was operated with 25–30 g/l riser solid concentration and about 1 kg/min circulation rate, resulting in fast-fluidized-bed flow conditions, which are characterized by solid back-mixing and strong fluctuations. The upper part of the riser is a quartz glass tube (0.5 m length), in which plasma was generated by alternatively coupling 500 W microwave (2.45 GHz) or 200 W rf power (13.56 MHz). Microwaves were coupled via a ring-shaped slotted antenna (four slots of 6 cm length) surrounding the quartz tube [27]. The active volume of MW coupling and plasma generation, defined as the tube cross-sectional area multiplied with the slot length, is only 75 cm^3. More than 10 W/cm^3 specific power is therefore reached in the center, causing a hot spot with up to 573 K gas temperature. The average particle temperature will stay below 373 K, but particles that remain extraordinarily long in the hot region can reach the gas temperature. In the case of rf coupling, two bent copper

Table 1
Experimental parameters during the plasma-CVD coating and resulting titania loadings

Experimental parameter	Catalyst code			
	RF10	MW10	MW30	MW100
Argon flow rate (mol h^{-1})	5.9	5.9	4.0	4.0
Precursor flow rate (mmol h^{-1})	5	5	7	20
Oxygen flow rate (mol h^{-1})	0.42	0.12	0.32	0.80
Process pressure (mbar)	8	8	4	4
Plasma excitation	RF	MW	MW	MW
Coating time (h)	2	2	4	4.5
Titania loading (mg g^{-1})	0.72	0.52	2.52	9.27
Film thickness (nm)[a]	9	7	32	116

[a] Calculated assuming "smooth" surface.

capacitor plates (30 cm length) were attached to the tube, enclosing 375 cm^3 active volume. The mean specific power was 0.53 W/cm^3, which is one order of magnitude lower than in the MW set-up. Therefore, the temperature field in the rf-source is very uniform and hot spots could not be detected. The local gas and solid temperatures are supposed to be well below 373 K at any position. The titanium precursor, $Ti(OtBu)_4$ (99.99%, Inorgtech Ltd.) was vaporized at 363–383 K in a bubbler using argon as carrier gas, mixed with oxygen and argon and fed into the reactor through a fine metal mesh at the bottom of the riser tube. Table 1 lists the process parameters used and the obtained TiO_2 loadings.

2.2. Titanium analysis

To determine the amount of deposited titania, the coated glass beads were placed in warm $(NH_4)_2SO_4$/conc. H_2SO_4 mixtures and the dissolved titania was then quantified either photometrically or by ICP-AES analysis. Two different dissolving conditions were applied: (a) a treatment with boiling 18 wt.% solution for 1 h, in which case a 0.1 mg/g titania contribution of the bare glass beads had to be subtracted; or (b) milder conditions, using an ultrasonic bath and a 10 wt.% solution at 313 K, in which case, the contribution of the bare beads was negligible (<1 μg/g). The latter conditions were employed to obtain time-resolved dissolution curves. The analytical results from the two different methods agreed within the experimental error.

2.3. Electron microscopy

To prepare TEM specimens, the embedded glass beads were mechanically thinned to 50 μm thickness and subsequently milled by a 10 kV Ar^+ ion beam at grazing angle (1–2°). Further details about the preparation procedure can be found in the literature [28]. The images were taken on a Philips CM20 transmission electron microscope operated at 200 kV acceleration voltage. SEM images were obtained on a JEOL JSM-35C instrument using 25 kV acceleration voltage. The SEM micrographs were taken on samples sputter-coated with a thin gold layer.

2.4. Surface analysis

X-ray photoelectron spectra (800 μm spot size) were collected on a physical electronics PHI 5700 XPS instrument using 350 W Al Kα irradiation. Pass energies of 93.9 eV for the surveys and 23.5 eV for the detail spectra were used; the elements were quantified using PHI sensitivity factors. Peak positions are referred to C 1s = 284.6 eV. Sputtering was performed using a 3 keV Ar^+ rastered ion beam at a standardized rate of 7.5 nm/min SiO_2. Time-of-flight secondary ion mass spectroscopy (ToF-SIMS) chemical maps were recorded on a physical electronics PHI 7200 imaging ToF-SIMS instrument using a 25 keV In^+ primary ion beam, 50 ns pulse width, 10 ns time per point and 200 frames. Images of 250 μm × 250 μm (256 pixels resolution, total ion dose 2.6 × 1012 ions cm^{-2}) and 50 μm × 50 μm raster widths (128 pixels resolution, 1.6 × 1013 ions cm^{-2}) were generated by integrating the Na^+, $28Si^+$, $(40Ca^+ + 40CaO^+)$, $(48Ti^+ + 48TiO^+)$ and ^{115}In signals.

2.5. Photocatalysis

The photocatalytic activity of the coated glass beads was evaluated in a "fully-irradiated" fluidized bed (FB) photoreactor operated in closed loop, by monitoring the decomposition rate of oxalic acid (as a model reactant), in aqueous solution (5×10^{-7} mol cm^{-3}) at 298 K. Water was "ultrapure", i.e. triply distilled, demineralized, free of organic content and filtered (0.2 μm membrane). Recycling systems were driven by variable speed peristaltic pumps (Masterflex,

model 2650MG). The temperature was kept constant (295 K) using a thermostatic bath.

The photoreactor was a multitube device: three concentric annuli and a tubular black light lamp (Philips TLD 18W/08; nominal output power: 18 W; superficial emission from 300 to 400 nm, with a peak at 350 nm) placed at its axis. The central annulus was the main reaction vessel. The outer one was an actinometric space to measure the exiting radiation outgoing from the reaction compartment, in order to monitor the satisfaction of fully irradiated photoreactor (FIP) conditions (i.e. all the particles along the light path are illuminated). The inner annulus was used as an IR filter. The bed expansion was fixed at 4.3 times the unexpanded bed, a level at which full irradiation of the entire reaction volume could be assured. The catalytic performance of the plasma-CVD films is compared to Degussa P-25 (∼75% anatase, $S_g \cong 50\,m^2\,g^{-1}$; $d_p = 30$–70 nm) which was immobilized onto Aldrich quartz sand (cat. no. 27473-9; $\rho = 2.4\,g\,cm^{-3}$; particle size: +50/−70 mesh) under comparable conditions (bed expansion = 3.8). The titania was immobilized in this case by humidifying a mixture of TiO_2 powder and a fraction of as-received sand (previously screened and washed with acetone). The mixture was then dried by evaporation under vacuum and calcined at 673 K for 12 h. Additional data on the experimental set-up, actinometric and reaction measurements and preparation of the reference sample are described in [8].

The titania-coated glass beads were tested as photocatalysts: (a) as deposited; (b) after being tested as deposited and then calcined at 713 K; and (c) after preconditioning/hydration in the photoreactor for 4 h, with subsequent calcination at 713 K. A portion of the calcined films were separated from the substrate in an ultrasonic bath, collected by filtration, dried and characterized by XRD in a Shimadzu XD-D1 diffractometer, using nickel filtered Cu Kα radiation. For comparison purposes, pieces of the coated quartz glass wall of the CFB plasma-CVD reactor were calcined and transmission spectra recorded using a Perkin-Elmer lambda 900 UV–VIS/NIR spectrometer.

3. Results and discussion

Photocatalytically active ultrathin titania films were deposited on a glass particle support by means of plasma-CVD. The reactor used combines a vacuum-operated CFB with a plasma deposition zone, as previously described [24]. This set-up has already been shown to generate homogeneous titania films on particles, so the purpose of the present investigation was to deposit optimized titania coatings of various thicknesses and to test their photocatalytic activity.

3.1. Film deposition and structure

The cross-sectional TEM image of a representative, individual titania-coated glass bead (Fig. 2) impressively demonstrates the unique potential of this coating technique. A conformal titania film of uniform thickness is clearly visible, virtually unaffected by collisions and free of delaminated areas. The accompanying plan-view SEM image confirms these observations and shows a homogeneous coating, which is entirely free of loose particles. Similar observations of the coating homogeneity were made using imaging ToF-SIMS, as discussed below. As further evident from both high-resolution TEM images and electron diffraction, the films are amorphous in the as-deposited state. Since the presence of the anatase TiO_2 phase is usually considered essential for photocatalytic activity [14], this means that a post-deposition calcination step is required in order to activate the catalyst. As shown by the XRD spectra of the stripped coating depicted in Fig. 3, mild calcination at 713 K for several hours was sufficient to induce the desired anatase formation. The films were well-adherent and mechanically stable. Only in the case of the thickest film, MW100, the TiO_2 loading was reduced by 35% after calcination plus two full catalysis cycles (see Table 2). This film damage may be attributed either to thermal stresses induced during the post-processing or to mechanical attrition during fluidization in the presence of water. As shown later by the ToF-SIMS images (Fig. 4), this damage seems to be due to homogeneous film wear, rather than to delamination of film patches.

Titanium analysis by chemical digestion shows that nearly 100% of the precursor were converted to TiO_2, independent of $Ti(OtBu)_4$ feed rate and plasma conditions. Taking into account the high specific energy input of more than 90 MJ/mol precursor (260 MJ/kg), full conversion was expected [29]. Within the investigated range of deposition rates, the precursor feed rate can thus be used to precisely adjust the titania loading.

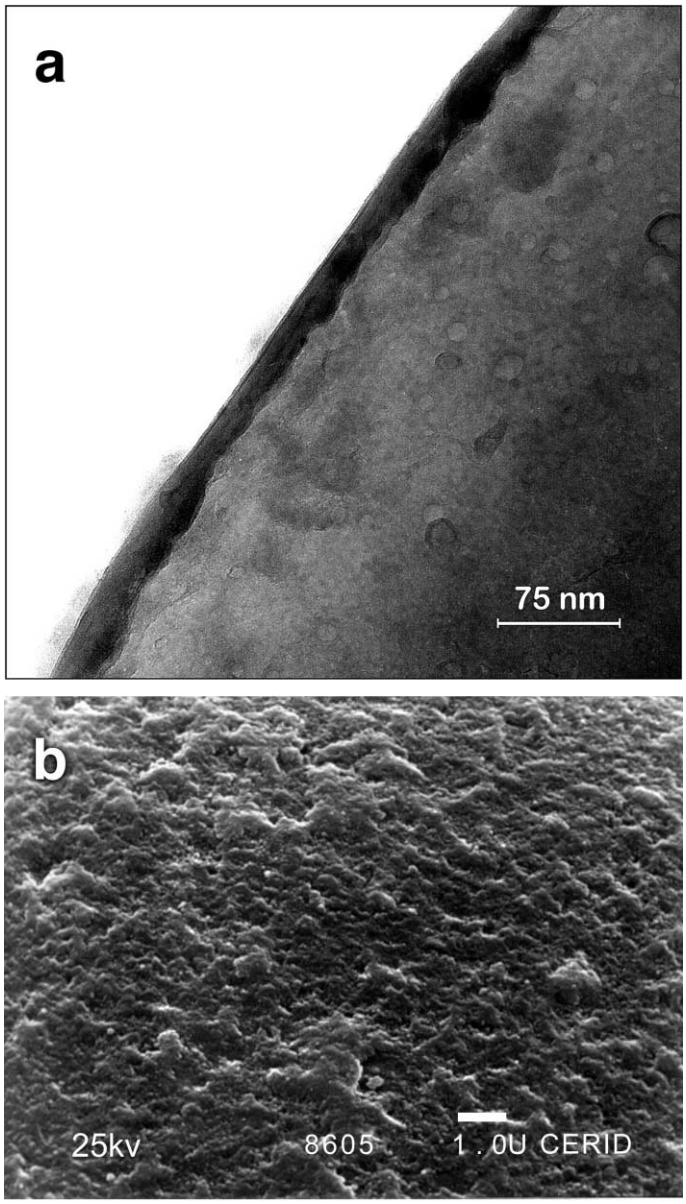

Fig. 2. (a) Cross-sectional transmission electron micrograph of a TiO_2 coating on a glass microbead (MW10, 0.52 mg/g load) deposited in a CFB by microwave plasma-CVD; (b) SEM micrograph of a TiO_2-coated glass microbead (MW30, 2.52 mg/g TiO_2 load) after 4 h of hydration and subsequent calcination at 773 K.

A small amount of titania, however, is always deposited on the reactor walls or lost by nanoparticle formation. On the other hand, it was found that up to 20% of the beads were trapped in stagnant zones and consequently remained completely uncoated (no aspect change). By analysis of beads sampled from the circulated part we found that these two effects balance to a nearly quantitative apparent precursor conversion rate.

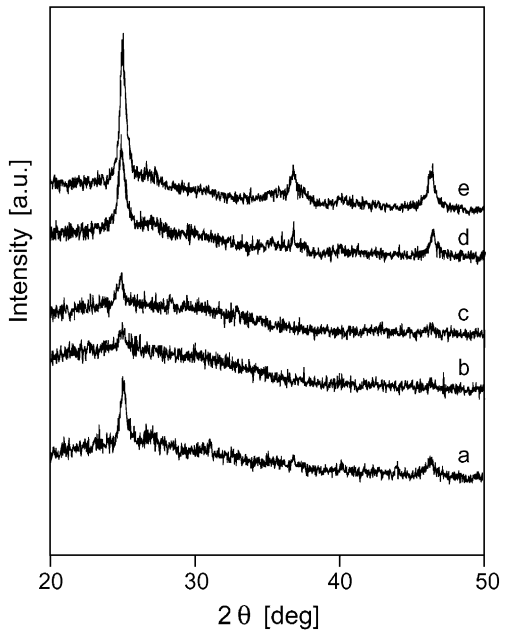

Fig. 3. XRD spectra of the stripped coatings of TiO_2 of the run catalysts: (a) MW10a; (b) MW30a; (c) MW30b; (d) MW100b (after previous hydration and calcination at 773 K); and (e) MW100a (after previous photocatalytic testing and subsequent calcination at 773 K) (see Table 2 for further details).

Besides the coating homogeneity per particle, the particle-to-particle homogeneity is an equally important issue for the later use of the coated material as a catalyst. The amount of titania deposited on an individual particle is basically proportional to its residence time in the deposition region. Although internal recirculation in the riser tube causes a wide distribution of residence time for a single loop, highly uniform coating is achieved through permanent removal and re-feeding during the process, comparable to the situation in a reactor cascade [30]. A suitable method to investigate the distribution of the deposited material is to look at the titania dissolution process in a time-resolved manner. Fig. 5 shows a typical dissolution curve obtained under mild conditions. Within the first few minutes, the topmost atomic layers (1–2 nm) are dissolved at a very high rate, which can be explained by the presence of loosely bound particulates and a high initial surface area. After this step, a constant dissolution rate of $D_f = 0.23$ mgTi/g/h is measured. In this regime, all beads are still coated. At prolonged treatment times, the coating has been completely dissolved and titania is now etched at a constant but smaller dissolution rate ($D_b = 0.01$ mgTi/g/h). Since the titanium background of the bare, acid-washed glass substrate was negligible (<0.3 μgTi/g/h), this has to be material that had diffused into the bulk silicate matrix during the deposition process. This diffusion may be enhanced both by ion bombardment in the plasma and by the microporosity introduced to the bead surface by the acid pre-washing. At the borderline between the two constant-rate regimes, portion Ψ of the beads is still covered with a remaining

Table 2
Film analysis and catalytic performance of fixed P-25 and coated glass beads

Sample	TiO_2 loading (mg g^{-1})	Calcination procedure	Crystal degree (XRD counts)[a]	P_C (%)	Initial reaction rate (mol cm^{-3} s^{-1} × 10^{12})
P-25/quartz	0.64	NA		87	25.2
RF10	0.72	None		68	2.5
RF10a	0.65	2.5 h[b]		68	9.5
MW10	0.52	None		76	6.0
MW10a	0.54	2.5 h[b]	3022	68	6.0
MW30	2.52	None		96	Nil
MW30a	2.21	2.5 h[b]	2230	96	6.2
MW30b	2.21	11 h[c]	2797	92	8.1
MW100	9.27	None		98	Nil
MW100a	5.92	2.5 h[b]	5224	98	17.8
MW100b	5.81	3 h[c]	3934	98	5.9

[a] I_{100} peak of anatase, $2\theta = 25.28^\circ$.
[b] After catalytic test, with UV irradiation.
[c] After 4 h of hydration in the FB, without UV irradiation.

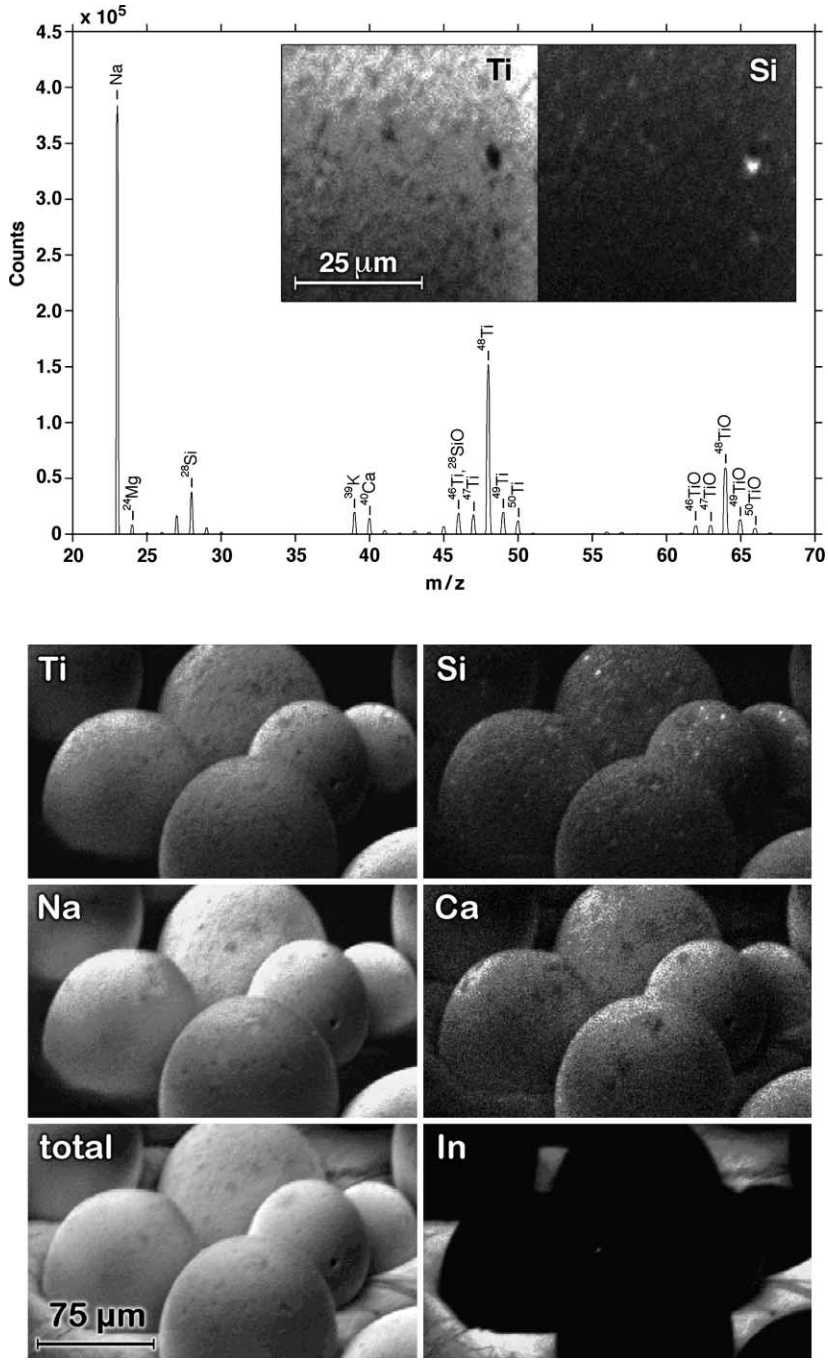

Fig. 4. ToF-SIMS images (25 keV In^+) of sample MW100a (5.92 mg/g TiO_2 load) after calcination and photocatalysis tests: (top) mass spectrum of an individual bead and 50 μm × 50 μm high-resolution map of that region (insert) illustrating the homogeneous coverage; (bottom) elemental survey maps of a group of beads showing the small number of film defects even after use in the FB photocatalysis reactor.

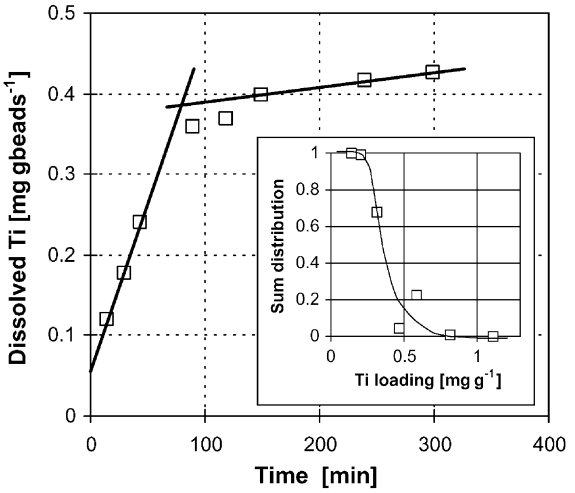

Fig. 5. Time-resolved dissolution curve of the TiO_2 coating (MW10, 0.52 mg/g TiO_2 load) under mild conditions (10 wt.% $(NH_4)_2SO_4$/concentration H_2SO_4 solution, in ultrasonic bath, 313 K) and calculated bead loading distribution (insert).

film, while other beads $(1 - \Psi)$ have already been completely stripped. The resulting dissolution rate is thus $D = \Psi D_f + (1 - \Psi) D_b$. The sharp bend of the curve shown in Fig. 5 clearly demonstrates the uniformity of the coating, as expected from the narrow residence time distribution [24]. The distribution of local titanium loading, corresponding to the local film thickness, can be estimated from the dissolution rate (insert of Fig. 5). Local titanium loading of this sample is basically between 0.2 and 0.6 mg/g, corresponding to 5–15 nm film thickness, with about 30% S.D. The titania loading values in Table 1 list the 'coating regime' titania contribution only, as this is the relevant measure for catalytic applications.

3.1.1. Deposition mechanism

The mechanism of the deposition process is very complex and it is not clear which is the favored reaction route. As illustrated in Fig. 6, the precursor is converted into the TiO_2 monomer by two competing pathways: plasma-fragmentation/plasma-oxidation and hydrolysis by water formed as a reaction product. Given the high specific plasma energy and relatively low precursor and water concentrations, plasma reactions are believed to be dominant. Despite the high gas velocity, notable gas back mixing has been reported for fast-fluidized beds [31]. This could allow some water to reach the lower part of the riser, causing hydrolysis reactions in this zone.

Film formation on the substrate particles may occur not only by heterogeneous CVD processes, but also by TiO_2 monomer polycondensation or by coagulation of ultrafine titania particles, which have formed by homogeneous nucleation. The dense and compact structure of the obtained films implies that the adsorption of both plasma-fragmented and unfragmented molecular species onto the particle surface, followed by oxidation or hydrolysis, dominates over particle-assisted film growth. At the low reactor pressures used, formation of fines is only expected to be favored during short periods, when flow fluctuations create areas of low solids concentration near the reactor center.

3.2. Surface analysis

The observed X-ray photoelectron spectroscopy (XPS) peak positions for the Ti 2p3/2 and O 1s signals, 458.7 and 529.8 eV, agree well with the literature values for titania [32]. In addition, both hydrocarbon and carbidic carbon was observed, which decreased

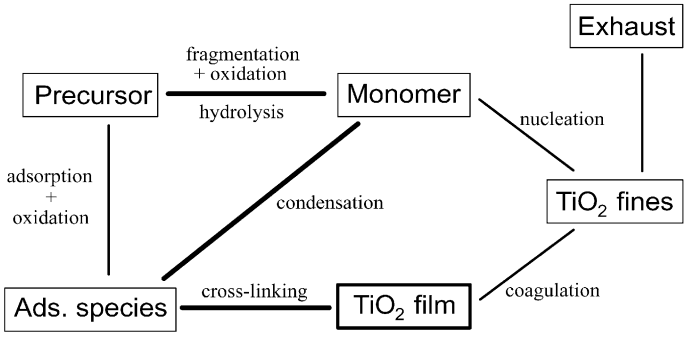

Fig. 6. Possible reaction steps during the plasma-CVD of titania thin films (according to Li et al. [20]).

Table 3
XPS chemical composition of titania layers of different thickness, 'as deposited' and after one and 2 min of sputtering with 3 keV Ar^{+}[a]

Sample	Sputter time (min)	Ti (at.%)	O (at.%)	C (at.%)	Si (at.%)	Ca (at.%)
RF10	0	19.48	68.10	5.32	6.88	0.22
	1	16.01	70.32	1.28	12.14	0.25
	2	11.86	71.63	0.89	15.32	0.30
MW10	0	21.26	64.73	7.83	6.07	0.12
	1	19.14	68.53	1.75	10.41	0.17
	2	14.87	69.24	1.29	14.36	0.24
MW30	0	20.18	63.64	11.31	4.50	0.36
	1	22.31	69.38	1.54	6.50	0.27
	2	21.15	69.34	1.59	7.60	0.32
MW100	0	21.13	63.69	10.37	4.81	0.00
	1	22.94	70.28	2.02	4.76	0.00
	2	23.35	69.11	1.08	6.18	0.28
MW100a[b]	0	18.39	63.06	12.74	5.27	0.55
	1	23.09	68.32	3.05	5.14	0.39
	2	24.45	68.39	1.95	4.76	0.45

[a] One minute Ar^{+} sputtering corresponds to 7.5 nm depth on a planar SiO_2 standard.
[b] Sample MW100a is equal to MW100, but after calcination and catalysis test.

to about 1 at.% after a brief sputtering (Table 3). In the light of the self-cleaning properties of titania [26] and the intense UV irradiation created by the plasma source, a low carbon content of the films had been expected. As shown in Fig. 7, silicon, sodium and calcium were also found at the particle surface, while two other glass constituents, K and Mg, could not be detected. The amount of incorporated silicon at the surface does not strongly depend on coating thickness and lies between 4.8 and 6.9 at.%. In contrast, increasing the titania film thickness decreased the surface sodium concentration from about 10 at.% for the thinnest films to about 5 at.%. Exact values for Na, however, cannot be given since especially after sputtering, the corresponding XPS signals could not reliably be deconvoluted from the interfering intense Ti and In peaks. Calcium was entirely suppressed by applying a coating of more than 100 nm thickness such as that of sample MW100, but was found to rediffuse to the surface after calcination (MW100a). After sputtering, the titanium signal remains constant for the two thicker coatings, MW30 and MW100. In contrast, Ti progressively decreases and the Si signal increases while sputtering the ultrathin coatings RF10 and MW10, indicating that the substrate surface becomes exposed once the films have been sputtered through.

For the chosen conditions, the XPS results did not show a significant influence of the frequency of plasma generation on film chemistry. Exposing the coated glass beads to aqueous oxalic acid during the photocatalysis test (sample MW100a) led to an increase in the detected carbon relative to the as-deposited state, sample MW100. This effect can be attributed either to chemisorbed oxalic acid or to surface roughening, which would lead to a less efficient sputter cleaning.

To investigate the spatial distribution of the catalyst and support elements within ultrathin films, imaging ToF-SIMS is the method of choice. This technique combines a spatial resolution of better than one micron with a low detection limit and a high surface sensitivity. We were particularly interested in the state of the coatings after particle calcination and dwelling in the fluidized bed of the photoreactor, as these 'run' samples provide information about the catalyst lifetime. A survey image of such a sample, MW100a, is shown at the bottom of Fig. 4. The titania loading of this initially more than 110 nm thick film (9.3 mg/g loading as deposited, MW100) had been reduced to 5.8 mg/g according to elementary analysis. Despite this significant film erosion, the ToF-SIMS images taken at various spots consistently show that the coating is still dense and uniform, for all the particles. The fact

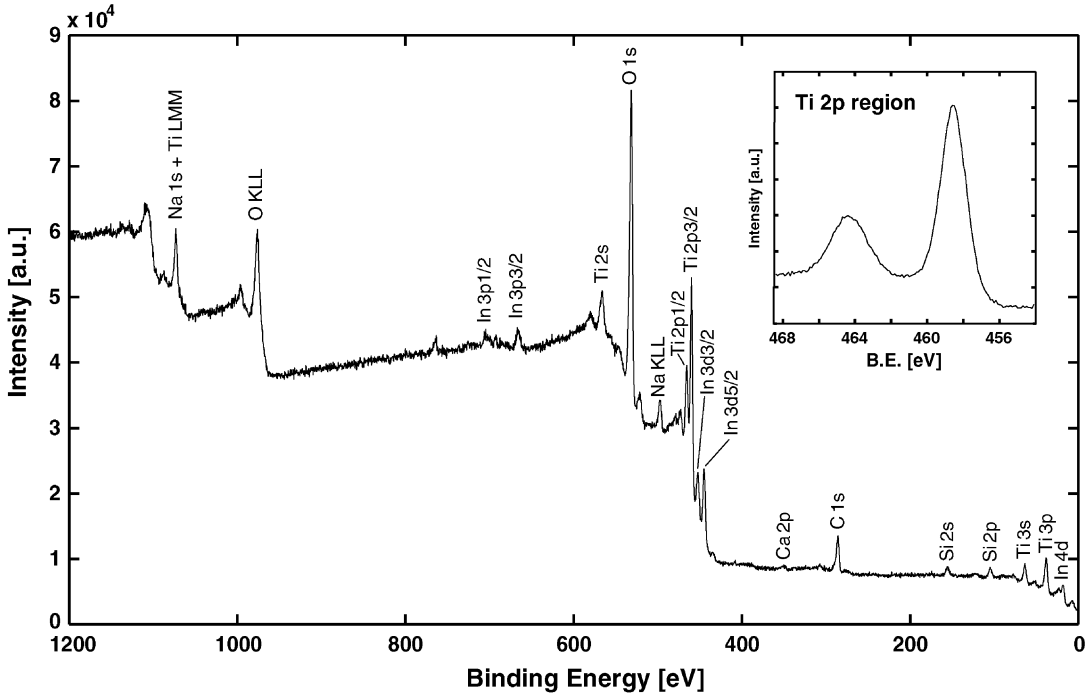

Fig. 7. XPS survey spectrum of the 'as deposited' MW30 coated glass beads (2.52 mg/g TiO_2 load) immobilized in indium foil.

that film delamination is not observed demonstrates the excellent film adhesion. However, there are occasional submicron-sized defect spots, where the titanium and silicon intensities behave complementary. These spots, one of which is more clearly depicted in the high-resolution image, insert of Fig. 4 (top), may be due to damage induced by particle–particle and particle–wall collisions in the fluidized beds of the coating and photocatalysis reactors. It is further obvious that, in accordance with the SEM images, almost no microparticles are attached to the sample surface. The corresponding mass spectrum shows sodium to be the most prominent impurity within the coating. As further evident from the survey chemical maps in Fig. 4, a small amount of silicon is also found homogeneously incorporated into the coating, as are alkali and alkaline earth elements such as K, Ca, and Mg. These glass-originating elements have diffused to the film either during film deposition, due to ion bombardment, or during sample calcination, by thermal diffusion.

Taking into account the XPS results and our earlier observations [24], it seems clear that the impurities are already present in the as-deposited films but further intensified by the calcination procedure. Nonetheless, as discussed below, poisoning even of the thin films was not severe enough to prevent photocatalytic activity. On the other hand, the thicker films performed generally better. This is not surprising in view of results obtained on titania coatings on float glass [26], which indicate that a minimum film thickness of 50 μm is required to prevent sodium ion poisoning of the photocatalyst. For optimum performance in our system, however, either choosing a more inert substrate particles or previous application of a buffer layer, such as SiO_2 [23,26], are required.

3.2.1. X-ray diffraction

Plasma-CVD titania without any additional heat-treatment is known to be amorphous [19]. However, the anatase peak ($2\theta = 25.28^\circ$) was detected in all MW samples after a mild calcination at 713 K. The samples grain size, determined from the peaks FWHM, was found to be of about 15 nm, in all cases. Since the amount of examined powder was equal for

all samples, and the FWHM did not change significantly, we believe that the peak intensity is proportional to the relative degree of crystallized material (Fig. 3 and fourth column of Table 2). The peak size increases with the film thickness, with UV irradiation followed by calcining, rather than just calcining (compare entries MW100a,b) and with longer calcination (compare entries MW30a,b). The relatively large peak of the thin film of MW10a is explained by the very slow film growth, which causes a more dense and compact film structure. Alternatively, incorporated silicon may promote anatase formation [33].

3.3. Optical properties of the PCVD titania films

Efficient light absorption is an essential requirement for photocatalytic activity. Since it is practically impossible to measure the optical properties of the film on the beads, parts of the coated quartz glass reactor wall were taken to measure the absorption spectra of the films. Fig. 8 shows the UV–VIS absorption spectrum of such a titania film, sampled 8 cm above the plasma source center after depositions MW30 and MW100 (after subtracting the substrate absorption). The effect of light scattering was fitted according to standard equations for spherical particles [34] and also subtracted. Best fit was achieved for about 30 nm mean scattering diameter. Compared to anatase, which reaches 50% absorbance at around 375 nm, we found a blue shift that is smallest (15–20 nm) after 723 K calcination. This is attributed to a smaller grain size [3] or to silicon incorporation (there are no other metal impurities in the quartz glass substrate). Even the 'as-deposited' films show strong absorption. Calcination at higher temperature moved the curve back to shorter wavelengths, possibly caused by rutile formation or further silicon diffusion. When the results are transferred to the film on the beads, some basic differences have to be considered. The glass beads have a much thinner film, they contain Na and Ca contamination and they pass by the total coating zone with axially changing conditions. Since similar results were achieved for films sampled from a more remote axial position (23 cm above the plasma source center), at least the transient deposition conditions are not considered to restrict transferability.

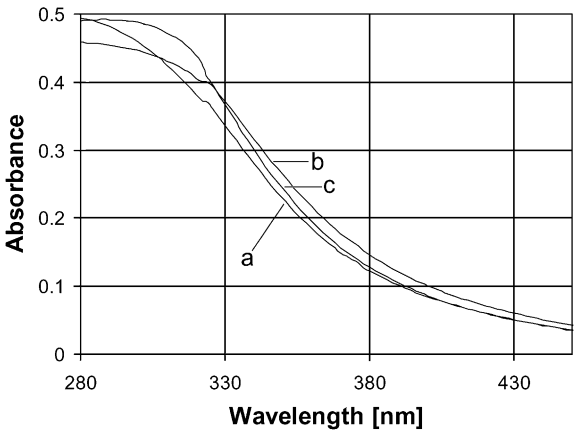

Fig. 8. UV–VIS absorption spectra of the titania film, sampled from the plasma-CVD quartz reactor wall: (a) as deposited (after MW30 and MW100 preparations) and after subsequent calcining at (b) 723 K; and (c) 873 K.

3.4. Photocatalytic performance

The amount of light absorbed by the film is proportional to the apparent captured power, P_C, in the photoreactor, which is defined as the difference between incident and outgoing radiation power per unit of reacting volume [8]. For the bare glass beads P_C equals 49%; for an equal mass of fluidized, bare quartz sand the measurement gave 58%. As shown in Table 2, P_C of the coated glass beads increases with increasing film thickness and slightly decreases after calcining. For comparable loading, it is lower than for P-25/quartz.

The catalytic performance of the coated beads, measured by the initial reaction rate of decomposition of oxalic acid, strongly correlates to the degree of crystallization and increases with thicker films, with UV pretreatment and with longer calcination time.

As expected [14], the amorphous 'as-deposited' films showed very low or no activity. The higher activity of as-deposited MW10 (relative to its RF10 counterpart) can be explained by the one order of magnitude higher power density of the microwave plasma. The resulting intense ion bombardment may alter the structure, particularly of the thinnest coatings, both during film growth [17] and, indirectly, by stronger substrate-film interactions. Doping of titania, especially with silica, has been shown not only to improve the film morphology [15], but also to render amorphous TiO_2 catalytically active [35]. However, we presently cannot say whether the presumably

greater interaction with the substrate of MW10 versus RF10 is beneficial or not. For example, MW10 does not improve as a photocatalyst after calcination (MW10a), whereas RF10 (prepared under milder plasma conditions) betters upon calcining. One possible explanation for this observation is that, while TiO_2 crystallization processes probably operate in both cases, thermal diffusion leads to unacceptable dopant levels in the more heavily pre-doped MW10 film.

The better photocatalytic performance of the thicker films, all of which were deposited in a MW plasma, reflects their higher resistance to impurity diffusion. However, even the thickest coating, MW100, keeps behind the performance of the immobilized P-25, whereas the captured power reaches very high levels. It is believed that the film crystallization is still not completed after calcining at 723 K, but also that *because* of this needed pretreatment Na- and Ca-incorporation has a negative impact. Higher calcination temperatures (e.g. 873 K) could improve the performance by completing the crystallization and reducing the amount of organic residues. Lastly, using quartz sand as substrate or adding a SiO_2 buffer layer between substrate and film would prevent the incorporation of glass-originating contaminants such as sodium.

4. Conclusions

Various loadings of amorphous TiO_2 were deposited on conventional glass beads by means of plasma-CVD. Variation of the plasma source from rf to microwave power had no significant influence on the chemical composition of the deposited material. Titania films with very low carbon levels but some incorporated silicon, sodium and alkaline earths were obtained, where less impurities were observed for thicker films. ToF-SIMS imaging and time-resolved dissolution of the films showed that the titania coatings are very uniform, both on a single particle and in terms of film thickness distribution among the particles. The presence of a dense and well-adherent thin film was further confirmed by transmission electron microscopy.

The thinnest films had some photocatalytic activity in the as-deposited state, possibly induced by the high specific power of the MW-plasma or silicon doping. The thicker films needed a post-deposition calcination at 723 K, associated with anatase formation, to achieve catalytic activity. Both the degree of crystallization and the activity were improved by applying thicker films, after UV irradiation-plus-calcining and/or longer calcining. All films showed good adhesion and abrasion resistance during the photocatalytic tests. The best plasma-CVD films were about 70% as efficient (per unit reactor volume) as the reference material, P-25 immobilized on quartz sand. Further improvement of the catalyst efficiency is expected by pre-coating a diffusion barrier layer or using inert support particles such as silica or alumina.

Acknowledgements

The ETH team thanks Irene Pfund for ToF-SIMS measurements, Dr. Imre Pozsgai for the TEM sample preparation and the Emil Barrell-Stiftung for financial support. The Argentine team thanks UNL, CONICET and ANPCyT for their continuous financial support. The technical assistance of Nora Pratta is also gratefully acknowledged.

References

[1] R.L. Pozzo, M.A. Baltanás, A.E. Cassano, Catal. Today 39 (1997) 219.
[2] J.A. Byrne, B.R. Eggins, N.M.D. Brown, B. McKinney, M. Rouse, Appl. Catal. B 17 (1998) 25.
[3] Z. Ding, X. Hu, G.Q. Lu, P.-L. Yue, P.F. Greenfield, Langmuir 16 (2000) 6216.
[4] E.-L. Lakomaa, S. Haukka, T. Suntola, Appl. Surf. Sci. 60/61 (1992) 742.
[5] K. Schrijnemakers, N.R.E.N. Impens, E.F. Vansant, Langmuir 15 (1999) 5807.
[6] L. Lei, H.P. Chu, X. Hu, P. Yue, Ind. Eng. Chem. Res. 38 (1999) 3381.
[7] N.B. Jackson, C.M. Wang, Z. Luo, J. Schwitzgebel, J.G. Ekerdt, J.R. Brock, A. Heller, J. Electrochem. Soc. 138 (1991) 3360.
[8] R.L. Pozzo, M.A. Baltanás, A.E. Cassano, Catal. Today 54 (1999) 143.
[9] M. Trillas, J. Peral, X. Domenech, J. Chem. Technol. Biotechnol. 67 (1996) 237.
[10] R.W. Matthews, Water Res. 25 (1991) 1169.
[11] X.-C. Guo, P. Dong, Langmuir 15 (1999) 5535.
[12] N. Serpone, E. Borgarello, R. Harris, P. Cahill, M. Borgarello, Solar Energy Mater. 14 (1986) 121.
[13] S. Seifried, M. Winterer, H. Hahn, Chem. Vap. Deposition 6 (2000) 239.

[14] B. Ohtani, Y. Ogawa, S. Nishimoto, J. Phys. Chem. 101 (1997) 3746.
[15] A. Matsuda, Y. Kotani, T. Kogure, M. Tatsumisago, T. Minami, J. Am. Ceram. Soc. 83 (2000) 229.
[16] M.L. Hitchman, J. Zhao, J. Phys. IV Fr. 9 (1999) 8–357.
[17] H. Yamashita, M. Harada, A. Tanii, M. Anpo, Proceedings of the Fifth International Conference on TiO_2 Photocatalytic Purification and Treatment of Water and Air, Ontario, Canada, 26–30 June 2000, p. 54.
[18] R. Pengcheng, T. Zhongke, L. Wenxiu, Chin. J. Chem. Eng. 4 (1996) 264.
[19] J.A. Ayllón, A. Figueras, S. Garelik, L. Spirkova, J. Durand, L. Cot, J. Mater. Sci. Lett. 18 (1999) 1319.
[20] C. Li, J. Han, Z. Zhang, H. Gu, J. Am. Ceram. Soc. 82 (1999) 2044.
[21] Y.A. Cao, X.T. Zhang, L.Q. Chong, Mater. Res. Soc. Symp. Proc. 497 (1998) 79.
[22] D. Korzec, T. Aumann, J. Engemann, M. Nakamura, Y. Hatanaka, Proceedings of the Seventh International Conference on Plasma Surface Engineering (ISPC), Garmisch-Partenkirchen (Germany), 17–22 September 2000, Paper Or 14:2.
[23] A. Fujishima, T.N. Rao, Proc. Indian Acad. Sci. Chem. Sci. 109 (1997) 471.
[24] M. Morstein, M. Karches, C. Bayer, D. Casanova, Ph. Rudolf von Rohr, Chem. Vap. Deposition 6 (2000) 16.
[25] J. Sheng, J. Karasawa, T. Fukami, J. Mater. Sci. Lett. 16 (1997) 1709.
[26] C.B. Greenberg, C.S. Harris, D.E. Singleton, J.P. Thiel, L.A. Kutilek, J. Szanyi, V. Korthuis, Int. Pat. Appl. WO 9841480 (1998).
[27] D. Korzec, F. Werner, R. Winter, J. Engemann, Plasma Sources Sci. Technol. 5 (1996) 216.
[28] S. Amelinckx, D. Vandyck, J. Van Landuyt, G. Van Fendeloo (Eds.), Handbook of Microscopy: Applications in Materials Science, Solid-State Physics and Chemistry, J. Wiley & Sons, N.Y., Vol. 3, 1996.
[29] M. Karches, Ph. Rudolf von Rohr, Proceedings of the Seventh International Conference on Plasma Surface Engineering (ISPC), Garmisch-Partenkirchen (Germany), 17–22 September 2000, Paper Or 01:6.
[30] M. Karches, Ch. Bayer, Ph. Rudolf von Rohr, Surf. Coat. Technol. 116–119 (1999) 879.
[31] J. Liu, J.R. Grace, H. Bi, H. Morikawa, J. Zhu, Chem. Eng. Sci. 54 (1999) 5441.
[32] J.F. Moulder, W.F. Stickle, P.E. Sobol, K.D. Bomben, in: J. Chastain (Ed.), Handbook of X-Ray Photoelectron Spectroscopy, Perkin-Elmer Co., Physical Electronics Division, Eden Prairie, MN 55344, USA.
[33] M.K. Akhtar, S.E. Pratsinis, S.V.R. Mastrangelo, J. Am. Ceram. Soc. 75 (1992) 3408.
[34] H.C. van de Hulst, Light Scattering by Small Particles, Dover Publishers, New York, 1981.
[35] H. Kisch, L. Zang, C. Lange, W.F. Maier, C. Antonius, D. Meissner, Angew. Chem. 110 (1998) 3201; Angew. Chem. Int. Ed. 37 (1998) 3034.